

61(2), pp. 224-230, 2017

<https://doi.org/10.3311/PPee.9737>

Creative Commons Attribution 

Barna Csuka^{1*}, Zsolt Kollár¹

RESEARCH ARTICLE

Received 14 July 2016; accepted after revision 09 January 2017

Abstract

In this paper we present parameter estimation methods for IEEE 802.11ad transmission to estimate the frequency offset value and channel impulse response. Furthermore a less known low complexity signal processing architecture – the Recursive Discrete Fourier Transform (R-DFT) – is applied which may improve the estimation results. The paper also discusses the R-DFT and its advantages compared to the conventional Fast Fourier Transform.

Keywords

WiGig, 802.11ad, R–DFT, parameter estimation, real-time measurement

1 Introduction

THE 802.11 standards of IEEE [1] describe the Wireless Local Area Networks (WLAN), which were designed originally for temporary data transmission between a main network device and some users with high network coverage. Nowadays requirements are changing, we require a continuous connection with Gbit/s data transfer rate and very low latency, furthermore the network should be decentralized.

IEEE serves the users needs through the development of the 802.11 standards (802.11b/g/n), but these improved solutions can not comprehensively address the following main problem: we will always have more and more electronic devices and a growing demand for digital content as well.

The IEEE 802.11ad standard operates in the yet rarely used 60 GHz frequency band with a bandwidth of 2 GHz [2]. The absorption of the electromagnetic waves is very high in air at 60 GHz and the effective antenna size is much smaller than at 2.4/5 GHz, so the range of the network is limited, to ca. 10-15 m. Therefore the aim of the standard's developers is to substitute the indoor wired and wireless data transmission between short range home devices.

Wireless transmissions using high data rates call for fast and accurate parameter estimation for compensation of the imparities such as frequency and phase offset or fading effects caused by the radio channel. Devices operating at higher frequencies – e.g. at 60 GHz in 802.11ad – require algorithms with low complexity and high precision for reduced power consumption and elevated data rates.

This paper focuses on the application of the Recursive Discrete Fourier Transform (R–DFT) for signal processing in digital data communication, which is a less known structure for calculating the Discrete Fourier Transform (DFT) of a signal sequence in a real-time manner [3, 4]. In contrast with conventional DFT filter structure [5] which can be unstable due to the quantization errors, this method is robust against stability issues.

Until now the R–DFT structure was primary used for measurement purposes [6, 7]. For wired and wireless communication applications, especially for Orthogonal Frequency Division Multiplexing (OFDM), the most frequently used

¹ Department of Broadband Infocommunications and Electromagnetic Theory, Faculty of Electrical Engineering and Informatics, Budapest University of Technology and Economics, 1521 Budapest, P.O. Box 91, Hungary

* Corresponding author, e-mail: csuka@hvt.bme.hu

solution for spectral analysis and parameter estimation is the Fast Fourier Transform (FFT). Despite the FFT being the most commonly used algorithm, some solutions, which employ two kinds of R-DFT, have already been presented for wireless communication applications: one based on the Goertzel algorithm [8] and the other one based on the observer theory [9], which is applied in this paper.

The FFT operates in a block by block manner, it calculates the N point spectrum from N time domain samples. Although FFT and R-DFT provide the same results after N incoming data, the R-DFT gives results through point by point calculation. This means that the transients can be also used for estimation and calculation in some special cases.

In this paper, two parameters are estimated: the frequency offset and the Channel Impulse Response (CIR). First, we present the known methods to estimate these parameters, and then we give extended solutions. The frequency offset estimation suggested by Moose uses the FFT [10]. Our procedure uses the method of Moose as well, but the FFT is substituted by R-DFT, so the variance of the estimation becomes lower. The channel estimation method is given for transmissions where complementary sequences are applied [11, 12]. The conventional solution calculates correlations [13], and the sum of the correlations give the CIR. Our applied method uses the Fourier Transform, which provides similar results as the correlator, but it can be more accurate in some applied scenarios.

The theoretical methods for frequency offset and CIR estimation are validated by applying them to the 802.11ad standard [2] as a case study. The 802.11ad contains Golay complementary sequences [11], for which the investigated estimation methods work effectively and they are comparable.

The paper is organized as follows. Section 2 gives a brief review of the 802.11ad standard. Section 3 introduces the R-DFT and the investigated parameter estimation methods. Section 4 presents the simulations (which were created in Matlab) and their evaluation. Finally, Section 5 draws the conclusions.

2 IEEE 802.11AD

2.1 About WiGig

The first version of the WiGig (WiGig 1.0) appeared in 2009, which was followed by the final version in 2011 (WiGig 1.1). The IEEE adopted this standard in the IEEE 802.11 standard family as 802.11ad, and WiGig became the part of the IEEE 802.11-2012 standard.

After the standardization, the Fast Session Transfer (FST) protocol was defined, which allows devices to change automatically between the different WLAN frequencies: 2.4, 5 and 60 GHz. The WiGig standard defines the wireless version of several wired bus system: Wireless Bus Extension (instead of PCIe), Wireless Serial Extension (instead of USB), Wireless Display Extension (instead of HDMI and DisplayPort) and Wireless SDIO Extension (instead of SDIO). The main

advantage of these solutions is that the connection is wireless, but the connector interface remains same as for the wired version. The first chipset, which supports the 802.11ad, was the 6100 family of Wilocity, which was followed by the 6200 and 6300 family, the last one is designed for mobile devices. The first 802.11ad-capable notebook was created by Dell, which was based on the products of Wilocity. This notebook (Dell 6430u) communicates with a docking station (Dell D5000) using 802.11ad. The first 802.11ad-capable routers were designed by TP-Link (Talon AD7200), Acelink (BR-6774AD) and Netgear (Nighthawk X10), these devices appeared in 2016.

2.2 Physical layer

The baseband bandwidth of WiGig is 2 GHz, which is converted up to 60 GHz carrier frequency. The theoretical maximum of the data transfer rate is 7 Gbit/s. The Radiocommunication Sector of the International Telecommunication Union (ITU-R) defined 4 channels between 57-66 GHz each having a bandwidth of 2.16 GHz. One of these channels – the second channel with a carrier frequency of 60.48 GHz – is available as an unlicensed band all over the world, therefore it is defined as the default band in the WiGig standard [2], as shown in Fig. 1. The compulsory spectral mask for a transmission channel can be seen in Fig. 2 [14, 15].

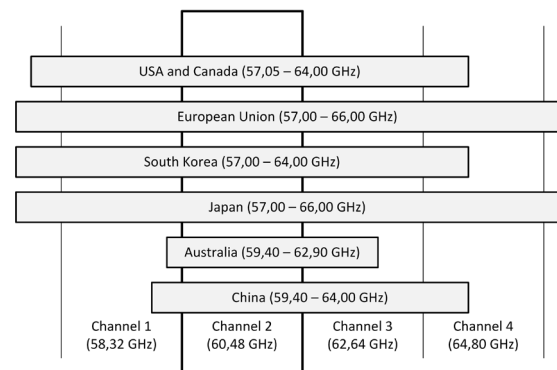


Fig. 1 Channels in the 57-66 GHz band and their frequencies

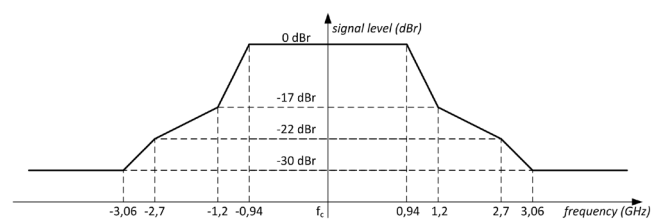


Fig. 2 Spectral mask of a channel according to the carrier frequency

In the physical layer, single carrier and OFDM transmission are applied as waveforms. The baseband signal of a single carrier (SC) transmission is a complex, digital modulated signal, where the following three modulation schemes are supported: BPSK, QPSK and 16-QAM. In case of OFDM transmission, the baseband signal (called as OFDM-symbol) is created using a 512-point inverse FFT, and 355 subcarriers are used for

transmitting data applying one of the following four modulation schemes: QPSK, SQPSK, 16- or 64-QAM [1].

2.3 Frame format

The data packet (shown in Fig. 3) has the following parts in SC mode: preamble, header, data and beamforming training sequences. In our paper, only the preamble is used for parameter estimation, so it is presented in details hereinafter [2].

Preamble		Header	Data	Beamforming training
STF	CEF			

Fig. 3 Packet structure of 802.11ad

The preamble contains a Short Training Field (STF) for synchronization and a Channel Estimation Field (CEF). These fields are built up from complementary Golay sequences [11], [12], which have 4 types: Golay-A (Ga), Golay-B (Gb) and their negated variants. These sequences are 128 samples long, so the following notations are applied: Ga_{128} , $-Ga_{128}$, Gb_{128} and $-Gb_{128}$. They can be generated using a Golay-generator, which is presented in Appendix A, where the necessary settings are also specified for $N = 128$.

The structure of the STF and CEF is shown in Fig. 4. The STF is a periodic signal with 20 Ga_{128} sequences and it is terminated by a $-Ga_{128}$ field. The CEF is not periodic, but it contains complementary sequences for the channel estimation. It has three main parts: a Golay-U (Gu_{512}), a Golay-V (Gv_{512}) (both consisting of Ga_{128} and Gb_{128} sequences) and a closing $-Gb_{128}$ sequence.

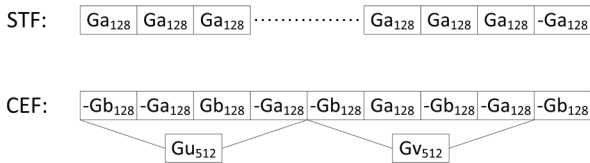


Fig. 4 Structure of STF and CEF

The preamble for an OFDM transmission is almost the same, only the order of Gu_{512} and Gv_{512} is reversed. Therefore the parameter estimation methods, which are presented in this paper, can be used without modification for OFDM transmission as well.

3 Theory

3.1 Recursive Discrete Fourier Transform

The conventional DFT and its implementation, the FFT operate only in a block by block manner. The application has to wait for a block of N incoming data to calculate the N -point spectrum, and refresh the results of the measurements. This causes delays during the operation, while real-time applications need a solution which provides an N -long spectrum following each incoming data.

To provide continuous spectrum calculation, the Sliding Discrete Fourier Transform (S-DFT) is applied [5], which is a filter bank based on a Lagrange structure. The S-DFT uses a moving average filter which includes complex resonators. The resonator modulates the signal by $e^{j2\pi\frac{k}{N}}$, that also gives the k -th spectral component at k/N center frequency, where sampling frequency is unity and k is the ordinal of the actual filter. If N filters are used, then the total N -point spectrum is given by the filter bank, and the result refreshes at each incoming data. The poles of this S-DFT are located on the unit circle, so the system is only marginally stable. If the applied arithmetic precision is finite, then the absolute value of resonators can be slightly smaller or larger than unity. If the poles are located outside the unit circle, the system is not going to be stable, the results will be divergent. If the poles are located inside the unit circle, then the results will converge to zero [5, 9].

Pécéli provides an alternative solution for spectrum calculation according to Hostetter's proposal [3, 4], the R-DFT, which is based on the observer theory. This model supposes that the measured signal ($x[k]$) is a linear combination of the elements of a basis system, as Fig. 5 shows.

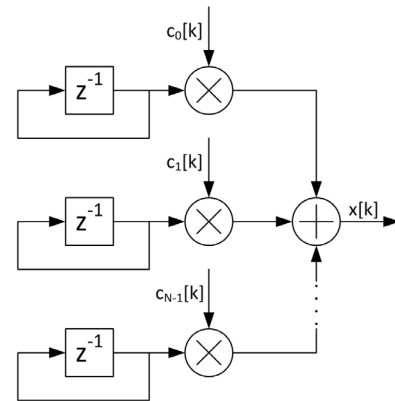


Fig. 5 Schematic structure of the signal generator

The observer (Fig. 6), which is responsible for the signal decomposition, has the following state variables: $\tilde{\mathbf{X}}[k] = (\tilde{\mathbf{X}}_0[k], \tilde{\mathbf{X}}_1[k], \dots, \tilde{\mathbf{X}}_{N-1}[k])^T$, and its system equation can be expressed as [4]:

$$\tilde{\mathbf{X}}[k+1] = \tilde{\mathbf{X}}[k] + \mathbf{g}[k]\mathbf{c}^T[k](\mathbf{x}[k] - \tilde{\mathbf{X}}[k]). \quad (1)$$

Pécéli proves the following 3 statements [4]:

- 1) the observer is convergent, so the error reaches zero in N steps if $\prod_{k=0}^{N-1} (\mathbf{I} - \mathbf{g}[k]\mathbf{c}^T[k]) = 0$, which is true, if $\mathbf{c}[k]$ and $\mathbf{g}[k]$ are basis/reciprocal basis systems;
- 2) the state variables of the observer ($\tilde{\mathbf{X}}[k]$) are the spectral components of the observed signal, if $\mathbf{g}_i[k] = \frac{1}{N} e^{-j2\pi\frac{k_i}{N}}$ and $\mathbf{c}_i[k] = e^{j2\pi\frac{k_i}{N}}$ so this observer calculates recursively the DFT;
- 3) this observer structure is equivalent to the Lagrange structure.

3.2 Comparison of FFT and R-DFT

If DFT is applied, then the most suitable method has to be chosen for the spectrum calculation. In this section, hardware requirements are compared.

The input data are complex, but the adders and multipliers calculate with real numbers. A complex addition requires only two real adders. The multiplication is more complex: it requires five real adders and three real multipliers. To store a complex number, two real memory cells are needed. The following requirements are calculated taking into account these values, and the applied arithmetic units are considered as real valued.

Duhamel compared the complexity of different FFT realizations [16]. From this paper, the most efficient solution, the Split-Radix FFT is taken for the comparison. Its requirements are proportional to $N \log_2 N$. By contrast, the R-DFT (Fig. 6) shows a linear dependence on N . It contains in each branch two complex multipliers, a complex adder and a complex memory cell. In addition, there is a complex adder at the input, and $N - 1$ complex adders at the output. The requirements for FFT and R-DFT are compared in Fig. 7 for $N = 2^4 \dots 2^{16}$.

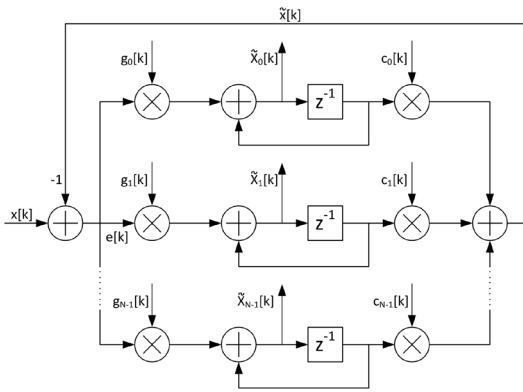


Fig. 6 Schematic structure of the observer based R-DFT

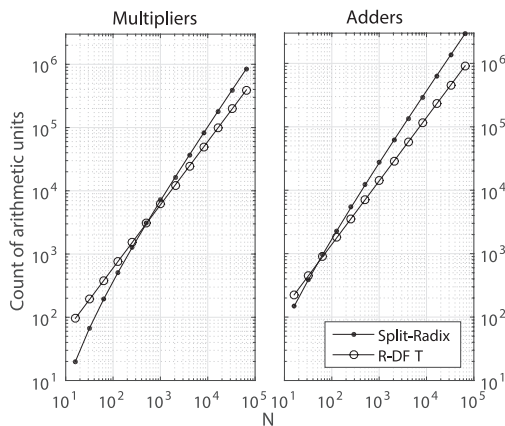


Fig. 7 Hardware requirements of DFT calculations depending on N

The FFT butterfly has $\log_2 N$ stages, which is equal to its latency. In contrast, the R-DFT has only a single stage, and latency is induced only by the pipelined structure of the arithmetic units in a branch. The calculations of R-DFT runs

parallel on individual branches. However, the R-DFT has a disadvantage, that it needs two memory cells per branch for the integrator to store the actual complex spectral value. As a result the R-DFT has an additional requirement of $2N$ memory cells.

3.3 Estimation of the frequency offset

The transmitter and the receiver are independent from each other, so the frequencies of their local oscillators may differ. In this case the received constellation points start to rotate on the complex plane with an $\omega_c = 2\pi\Delta f_c$ angular velocity, where Δf_c denotes the difference between the frequencies of the oscillators.

Moose showed [10] that the maximum likelihood estimate of Δf_c can be given by

$$\Delta \tilde{f}_c = \frac{1}{2\pi} \cdot \arctan \left(\frac{\sum_{i=0}^{N-1} \text{Im} \{ \mathbf{X}_{2,i} \bar{\mathbf{X}}_{1,i} \}}{\sum_{i=0}^{N-1} \text{Re} \{ \mathbf{X}_{2,i} \bar{\mathbf{X}}_{1,i} \}} \right), \quad (2)$$

where $\mathbf{X}_{1,i}$ and $\mathbf{X}_{2,i}$ is the i -th bin of the N -point DFT of two consecutive, identical transmitted data blocks, and $\bar{\mathbf{X}}$ marks the complex conjugate of \mathbf{X} . $\text{Re}\{\cdot\}$ and $\text{Im}\{\cdot\}$ denote the real and imaginary parts respectively.

3.3.1 Estimation by R-DFT

The N points R-DFT calculates the spectrum point by point, where N is the periodicity of the received data because of the convergence properties [4]. The procedure of Moose in Eq. (2) is adaptable, and $\Delta \tilde{f}_c$ is calculated for each incoming data. \mathbf{X}_2 is the latest estimated spectrum: $\mathbf{X}_2 = (\tilde{\mathbf{X}}_0[k], \tilde{\mathbf{X}}_1[k], \dots, \tilde{\mathbf{X}}_{N-1}[k])$. \mathbf{X}_1 should be the periodically shifted version of \mathbf{X}_2 , so \mathbf{X}_1 contains the former $k-N$ output values of the R-DFT: $\mathbf{X}_1 = (\tilde{\mathbf{X}}_0[k-N], \tilde{\mathbf{X}}_1[k-N], \dots, \tilde{\mathbf{X}}_{N-1}[k-N])$.

The calculated $\Delta \tilde{f}_c$ values have the same length as the input data. They show the change of frequency offset during transmission of N data bits, and this result is also useable to create a closed control loop to correct the frequency offset. If only a single offset value is required, the average of $\Delta \tilde{f}_c$ has to be calculated in two steps:

- 1) first, the offset values are filtered by a moving average filter of width M ;
- 2) the final $\Delta \tilde{f}_c$ is going to be the average of every M -th filtered offset value, which are independent from each other because of the moving average,

where M may differ from N . The output of this averaging gives the filtered, estimated value of $\Delta \tilde{f}_c$, which can be used to compensate the received signal.

3.4 Estimation of the CIR

The transmitted signal is affected by the radio channel, so it is necessary to apply a compensation filter. This filter's frequency response has to be the inverse of the channel frequency response (CFR). So either the CTF or CIR has to be known to perform this compensation. The estimated spectral values of

the incoming data are $\tilde{\mathbf{X}}$. The ideal spectral values (\mathbf{X}) have been calculated and stored previously as a reference.

The transfer function ($\tilde{\mathbf{H}}$) can be expressed in the following way using zero forcing for each subcarrier: $\tilde{\mathbf{H}}_i = \tilde{\mathbf{X}}_i/\mathbf{X}_i$. It is important to note that the spectral values (\mathbf{X}_i) may be zeros. To avoid the division by zero, the bin where $\mathbf{X}_i = 0$ has to be interpolated or replaced by the corresponding value of another CFR estimate.

This procedure is the same with R-DFT. As the last received sample of an N long block is retrieved, the R-DFT produces the DFT values of the block.

4 Simulations

4.1 Simulation of the radio channel

During the simulations, the transmitted packet is modulated by $\pi/2$ -BPSK modulation according to the 802.11ad standard [2]. In this simulation, only the baseband transmission is applied without up- and downconversion, but the effect of converting units is simulated. These units at the transmitter and receiver side are independent from each other, so the frequency of their oscillators may differ. This frequency difference may lead to a frequency offset error. The fading effect of the channel is simulated by a FIR filter and the noise of the channel is simulated by adding normally distributed random complex values to the transmitted signal. During the simulations only the investigated and estimated parameters have non-zero values, all other impairments are set to zero.

4.2 Frequency offset estimation

Equation (2) is given for OFDM transmission, but it can be further developed to be used for 802.11ad as well. \mathbf{X}_1 and \mathbf{X}_2 should be consecutive received Ga_{128} sequences from the STF. The estimated frequency offset can be calculated again for the consecutive Ga_{128} sequences, thereafter the estimated frequency offset values can be averaged. It is important that the first Ga_{128} block will not be used, because of the transients after the start of the transmission may distort the signal.

The first method is to apply the FFT, Fig. 8 shows the selection of the slices. In this case there are 14 pairs of Ga_{128} blocks (the first Ga_{128} are not used), so there are 14 estimated frequency offset values, which can be averaged.

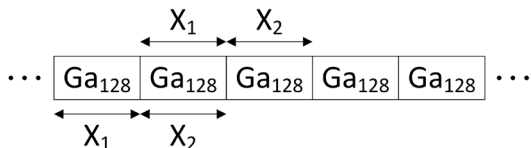


Fig. 8 Selected blocks for frequency offset estimation purposes

The second calculation is based on the previously presented R-DFT, and the method for this estimation is presented in Section 3.3.1, where N and M are 128 because of the periodic structure of the STF.

During the simulations, the signal-to-noise-ratio (SNR) is set between 0 and 40 dB in steps of 1 dB. At each SNR value, 25 transmissions are generated, and to each transmission $\Delta\tilde{f}_c$ is calculated. These 25 values are averaged, and also their variance is calculated. The result of these simulations is the variance depending on SNR, which is presented in Fig. 9. The Δf_c is chosen to be 0.15 and 0.35, but H_{ch} is considered to be ideal.

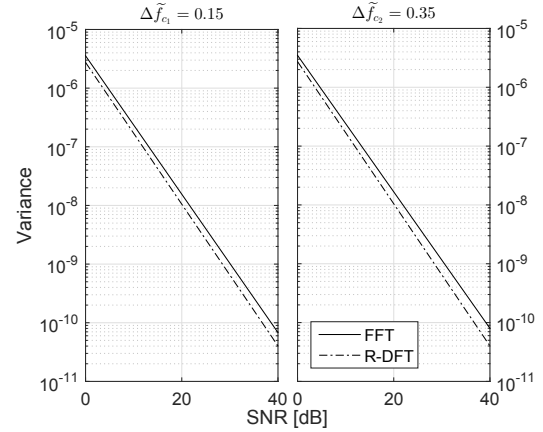


Fig. 9 Variance of estimated frequency offsets versus SNR

4.3 CIR estimation

In Section 3.4 the method for the channel estimation was presented, which is investigated in this section. The estimation is calculated by FFT and by R-DFT (where $N = 512$) to determine \tilde{H}_{ch} as the average of \tilde{H}_U and \tilde{H}_V . They provide the same result, so they are considered jointly as *FFT/R-DFT*.

New solutions are simulated as well: the extended Fourier Transforms. At first, the last $-Ga_{128}$ block of STF and the last $-Gb_{128}$ block of CEF are also used (see in Fig. 4 and 10), so the Gv_{512} and Gv_{512} are considered as a quasi-periodic signal. This means that \tilde{H}_{ch} is given by averaging 4 estimations with this extension. This provides a better result (called *Extended FFT/R-DFT*), because the added slices ($-Ga_{128}$ and $-Gb_{128}$) are independent of the previous estimations, so their variances can be reduced.

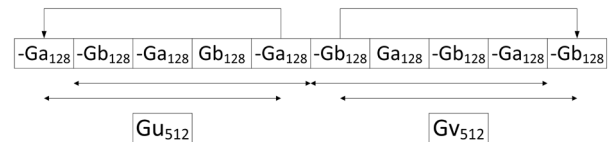


Fig. 10 CIR estimation based on the CEF structure

Another extension of the channel estimation is the usage of STF (called *With STF extended FFT/R-DFT*). The transfer functions of Ga_{128} are also calculated with $N = 512$, so zeros are padded to increase the length from 128 to 512, the results are then averaged.

During the simulations, SNR is set between 0 and 40 dB in steps of 2 dB. At each SNR-value, 25 transmissions are generated, and to each transmission \tilde{H}_{ch} and the CIRs are calculated.

These 25 values are averaged, and their variance is expressed. The variance of CIR depending on SNR is presented in Fig. 11. The ideal simulated CIR has a length of 1 and 2 samples, and no frequency offset is applied to the signal.

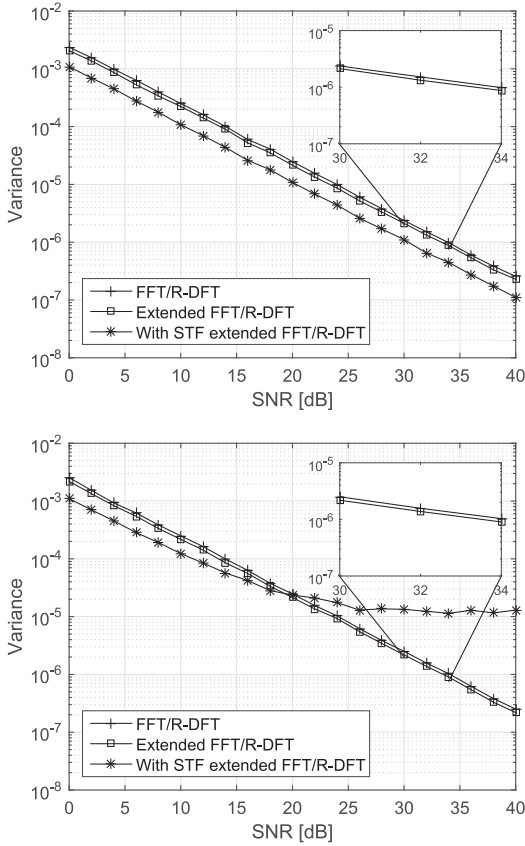


Fig. 11 Variance of estimated CIR (lengths are 1 and 2 samples) versus SNR

4.4 Evaluation of the simulations

In case of frequency offset estimation (Fig. 9), the results of Fourier Transform are used for the calculations. The variance of the estimated frequency offset is depending on the number of according to the in (2) calculated values. However, the FFT works blockwise, while the R-DFT gives its result to each input data, and it uses the transients as well, not only the stable states. It means that more estimation can be calculated, the averaging operates over more values, and in this case the variance of the results can be reduced. Fig. 9 shows, that R-DFT gives better estimation than FFT. Theoretically the FFT could have provided results as good as the R-DFT, and it could have been calculated after every incoming sample. But as it was mentioned, the FFT works in a block-by-block manner, which is not efficient for a point-by-point estimation.

For CIR estimation (Fig. 11) the conventional FFT and the proposed solution, the R-DFT give the same results with the same variances. With the extension of $G_{u_{512}}$ and $G_{v_{512}}$ sequences, the variance of the estimations can be reduced. On the other hand if the CFR is flat or the SNR is low, then better results could be obtained and it is beneficial to use the STF for

channel estimation as well for the frequency offset estimation. This method does not always decrease the variance depending on SNR. It is unable to estimate the DC-transfer of the channel from the $G_{a_{128}}$ sequences, because they do not contain any DC-component. As a result an error floor can be observed in the variance.

5 Summary

In this paper the IEEE 802.11ad standard is presented, which may be notable after the appearance of the first 802.11ad-capable routers. This wireless communication protocol has many new solutions to ensure high data transfer rate. In this paper, we have investigated high throughput parameter estimation methods based on the Fourier Transform.

We have shown parameter estimation methods for 802.11ad, where the R-DFT could be as efficient procedure as the FFT. For channel estimation, both methods give the same result with equal variance. For frequency offset estimation, the R-DFT can be better than FFT because it operates in a point-by-point manner. This means that the transients may be also used for the estimation, this additional data gives a wider averaging range, thus it reduces the variance of the estimation.

Appendix A

Golay Complementary Sequences

Golay introduced such binary sequences [11] that two of them are complementary to each other. This means, that the sum of their autocorrelations is zero, except when the time index, k is zero.

Budišin gave the following algorithm [12], which can generate the corresponding Golay sequences with a length of N :

$$a_0[k] = b_0[k] = \delta[k] \quad (3)$$

$$a_n[k] = a_{n-1}[k] + W_n \cdot b_{n-1}[k - D_n] \quad (4)$$

$$b_n[k] = b_{n-1}[k] - W_n \cdot a_{n-1}[k - D_n], \quad (5)$$

where $\delta[k]$ denotes the Kronecker delta function, n is the number of iterations. W_n contains the amplifying coefficients, and D_n is the length of delay elements.

For the case of $N = 128$, the following values are applied to generate the standard sequences in $n = 7$ steps for 802.11ad [2]:

$$\mathbf{W} = [-1, -1, -1, -1, +1, -1, -1],$$

$$\mathbf{D} = [1, 8, 2, 4, 16, 32, 64].$$

This work was supported by the János Bolyai Research Fellowship of the Hungarian Academy of Sciences.

References

- [1] "IEEE Standard for Information Technology – Telecommunications and information exchange between systems Local and Metropolitan Area Networks – Specific requirements Part 11: Wireless LAN Medium Access Control (MAC) and Physical Layer (PHY) Specifications." *IEEE Std 802.11-2012 (Revision of IEEE Std 802.11-2007)*, Mar. 2012.
- [2] "IEEE Standard for Information Technology – Telecommunications and information exchange between systems Local and Metropolitan Area Networks – Specific requirements Part 11: Wireless LAN Medium Access Control (MAC) and Physical Layer (PHY) Specifications – Amendment 3: Enhancements for Very High Throughput in the 60 GHz Band." *IEEE Std 802.11ad-2012 (Amendment to IEEE Std 802.11-2012, as amended by IEEE Std 802.11ae-2012 and IEEE Std 802.11aa-2012)*, Mar. 2012.
- [3] Hostetter, G. "Recursive discrete Fourier transformation." *IEEE Transactions on Acoustics, Speech, and Signal Processing*. 28(2), pp. 184-190. 1980. <https://doi.org/10.1109/TASSP.1980.1163389>
- [4] Péceli, G. "A common structure for recursive discrete transforms." *IEEE Transactions on Circuits and Systems*. 33(10), pp. 1035-1036. 1986. <https://doi.org/10.1109/TCS.1986.1085844>
- [5] Jacobsen, E., Lyons, R. "The sliding DFT." *IEEE Signal Processing Magazine*. 20(2), pp. 74-80. 2003. <https://doi.org/10.1109/MSP.2003.1184347>
- [6] Nagy, F. "Measurement of signal parameters using nonlinear observers." *IEEE Transactions on Instrumentation and Measurement*. 41(1), pp. 152-155. 1992. <https://doi.org/10.1109/19.126651>
- [7] Orosz, G., Sujbert, L., Péceli, G. "Analysis of Resonator-Based Harmonic Estimation in the Case of Data Loss." *IEEE Transactions on Instrumentation and Measurement*. 62(2), pp. 510-518. 2013. <https://doi.org/10.1109/TIM.2012.2215071>
- [8] Lai, S. C., Juang, W. H., Lee, Y. S., Lei, S. F. "High-performance RDFT design for applications of digital radio mondiale." In: IEEE International Symposium on Circuits and Systems, 2013, Beijing, China, May 19-23, 2013, pp. 2601–2604. <https://doi.org/10.1109/ISCAS.2013.6572411>
- [9] Varga, L., Kollár, Zs. "Low complexity FBMC transceiver for FPGA implementation." In: Radioelektronika, 2013 23rd International Conference, Pardubice, Czech Republic, Apr. 16-17, 2013, pp. 219-223. <https://doi.org/10.1109/RadioElek.2013.6530920>
- [10] Moose, P. H. "A technique for orthogonal frequency division multiplexing frequency offset correction." *IEEE Transactions on Communications*. 42(10), pp. 2908-2914. 1994. <https://doi.org/10.1109/26.328961>
- [11] Golay, M. J. E. "Complementary series." *IRE Transactions on Information Theory*. 7(2), pp. 82–87. 1961. <https://doi.org/10.1109/TIT.1961.1057620>
- [12] Budišin, S. Z. "Efficient pulse compressor for Golay complementary sequences." *Electronics Letters*. 27(3), pp. 219-220. 1991. <https://doi.org/10.1049/el:19910142>
- [13] Lei, M., Huang, Y. "CFR and SNR Estimation Based on Complementary Golay Sequences for Single-Carrier Block Transmission in 60-GHz WPAN." In: IEEE Wireless Communications and Networking Conference, 2009, Budapest, Hungary, Apr. 5-8, 2009. pp. 1–5. <https://doi.org/10.1109/WCNC.2009.4917623>
- [14] *Wireless LAN at 60 GHz – IEEE 802.11ad Explained*, Agilent Technologies, 2013. URL: <http://cp.literature.agilent.com/litweb/pdf/5990-9697EN.pdf>
- [15] Schultz, B. "802.11ad – WLAN at 60 GHz – A technology introduction." Rohde & Schwarz, 2013. URL: https://cdn.rohde-schwarz.com/pws/dl_downloads/dl_application/application_notes/1ma220/1MA220_1e_WLAN_11ad_WP.pdf
- [16] Duhamel, P. "Implementation of "Split-radix" FFT algorithms for complex, real, and real-symmetric data." *IEEE Transactions on Acoustics, Speech and Signal Processing*. 34(2), pp. 285-295. 1986. <https://doi.org/10.1109/TASSP.1986.1164811>